Research Article | Vol. 10, No. 10 / 1 October 2020 / Optical Materials Express 2425
Optical Materials EXPRESS

Temperature dependent spectroscopic study of Yb^{3+}-doped $KG(WO_4)_2$, $KY(WO_4)_2$, $YAlO_3$ and $YLiF_4$ for laser applications

JÖRG KÖRNER,[1,2,*] MATHIAS KRÜGER,[3,4] JÜRGEN REITER,[1,2] ANDREAS MÜNZER,[3,4] JOACHIM HEIN,[1,2] AND MALTE C. KALUZA[1,2]

[1] *Institute of Optics and Quantum Electronics, Friedrich-Schiller University, Max-Wien Platz 1, 07743 Jena, Germany*
[2] *Helmholtz Institute Jena, Fröbelstieg 3, 07743 Jena, Germany*
[3] *Ludwig-Maximilians University Munich, Am Coulombwall 1, 85748 Garching, Germany*
[4] *Max-Planck-Institute of Quantumoptics, Hans-Kopfermann-Str. 1, 85748 Garching, Germany*
[*] *joerg.koerner@uni-jena.de*

Abstract: We present a study on temperature dependent spectroscopic data for Yb:KGW, Yb:KYW and Yb:YLF between 80 K and 280 K and Yb:YAP between 100 K and 300 K. Absorption and emission cross sections are determined. The latter ones are obtained by using a combination of the McCumber relation and the Füchtbauer-Ladenburg equation. Fluorescence lifetimes are measured within a setup optimized for the suppression of re-absorption and compared to the radiative lifetimes calculated from the previously determined cross sections to cross check the validity of the measurements. The cross sections are evaluated with regard to the materials' potential for supporting the generation of ultra-short laser pulses, low quantum defect lasing and requirements for suitable diode laser pump sources.

1. Introduction

During the last two decades diode pumped solid state lasers based on ytterbium doped gain media have demonstrated outstanding performance and efficiency. Non-birefringent materials like yttrium aluminum garnet ($Y_3Al_5O_{12}$, YAG) and CaF_2 are widely used a host material for the threefold positive ytterbium ions (Yb^{3+}). Besides these materials, birefringent hosts, especially the two tungstates potassium gadolinium tungstate ($KGd(WO_4)_2$, KGW) and potassium yttrium tungstate ($KY(WO_4)_2$, KYW also have a long history as gain media, particularly for the generation of ultra-short pulses [1–3] and their amplification [4]. The success of these materials is strongly linked to their broad emission spectra and relatively high emission cross sections.

Like in other Yb^{3+}-doped gain media, the relatively low quantum defect is coincident with a significant overlap of the absorption and emission bands, which causes re-absorption. In laser operation, however, this limits the gain and the efficiency, that can be obtained. Re-absoprtion, can - to some extent - be suppressed by operating the laser medium at cryogenic temperatures. Also the thermo-mechanical properties become more favorable at lower temperatures [5]. Therefore, tungstates have already been used quite early in combination with cryogenic cooling designs [6] to improve their performance.

Besides the two tungstates also yttrium aluminum perovskite ($YAlO_3$, YAP) enables the generation of ultra-short pulses [7] due to a broad emission band, but the cross sections are comparably small.

Another well known birefringent ytterbium host material suitable for the application in ultra-short pulse lasers is yttrium lithium fluoride ($YLiF_4$, YLF) (cf. e.g. [8,9]). It also features a broad emission band but in comparison to the other mentioned materials a long fluorescence lifetime of ≈2 ms.

#398740 https://doi.org/10.1364/OME.398740
Journal © 2020 Received 27 May 2020; revised 29 Jul 2020; accepted 7 Aug 2020; published 8 Sep 2020

Optical Materials EXPRESS

Besides the usability for ultra-short pulse lasers, another attribute that is common among the mentioned materials is that their emission spectra exhibit peaks near 1000 nm. This allows for the operation with low quantum defect and therefore low heat-load when pumped around ≈940-980 nm with commonly used diode laser pump sources. Such an operation scheme is especially sensitive on temperature due to the strong re-absorption at the lasing wavelength. Furthermore, such lasers often need to be operated at cryogenic temperatures [10]. Due to their, for ytterbium doped media, untypically large cross sections such operation could be easier maintained with the laser materials mentioned here rather than e.g. with Yb:CaF_2 that was used in a similar scheme in [11].

To develop laser systems based on these materials, a reliable data basis is crucial. Especially in the case of pulse pumped laser amplifiers, which mostly operate under small signal gain conditions, even small deviations in the input data for simulations can cause significant differences of the results. Therefore, temperature dependent data especially for cryogenically cooled systems is needed. Nevertheless, the current data basis on the mentioned materials is quite sparse and often limited to room temperature spectra or singular measurements at 80 K.

In this work we present a detailed spectroscopic study on these materials to fill this gap. Cross sections are determined within the temperature range from 80 K to 280 K using a proven work flow and an optimized setup for diminishing the influence of re-absorption, which we also used in our previous works on Yb^{3+}-doped gain media [12,13]. Also measurements for the fluorescence lifetime are presented, which are used to validate the determined cross sections.

The results are discussed in the following with respect to the impact on the laser performance and compatibility with common laser diode technology as the pump source.

2. Setup and data processing

All samples presented in this work were prepared by commercial suppliers for laser material. For Yb:KGW (*FEE GmbH*) and Yb:KYW (*EKSMA Optics, UAB*) we used two crystals of each type, one prepared with N_g cut, the other with N_p-cut, to be able to access all three polarization orientations. In case of Yb:YAP (*Scientific Materials by FLIR Systems*) four crystals were used, two with b-cut and two with c-cut. For the naming of the axes we applied the Pnma notation. The two samples for each cut direction had thicknesses of 10 mm and 2 mm, respectively, to increase the absorption measurement's dynamic range. The thick samples were used for the measurements in the low absorption spectral parts, while the thin samples were used in the high absorption areas. The results for Yb:YLF were obtained from a single sample having the π-axis within the cut plane. Since this is a uni-axial crystal, both polarization axes could be investigated. An overview of the samples' parameters is given in Table 1.

Table 1. Parameters of the investigated samples: c_{dop} ... doping concentration, n ... mean refractive index, d ... thickness.

host	c_{dop}	d	n
KGW	$3.15 \cdot 10^{20}$ cm^{-3} (5 at.%)	1.5 mm	2.0 [14]
KYW	$3.19 \cdot 10^{20}$ cm^{-3} (5 at.%)	2.2 mm (N_p) 1.4 mm ($N_{g,m}$)	2.0 [15]
YAP	$1.97 \cdot 10^{20}$ cm^{-3} (1 at.%)	10 mm 2 mm	1.956 [16]
YLF	$14.0 \cdot 10^{20}$ cm^{-3} (10 at.%)	4 mm	1.455 [16]

Optical Materials EXPRESS

The Setup and data processing routines have already been described in [12,13]. Here, we only give a short description of the evaluation routines.

The setup for the measurements is shown in Fig. 1. The fiber coupled white light source WLS1000 (WLS, *Bentham Instruments Ltd.*) is focused with a spherical mirror (SM) and propagates through the sample. The transmitted light is collected with a second spherical mirror, which produces a second focal spot. This second focus is then re-imaged to the entrance of the fiber connected to the analysis equipment using two parabolic mirrors (PM) in a 4f-telescope setup. All spectral measurements were done with an AQ-6315A/B (*ANDO Electric Co. Ltd.*) optical spectrum analyzer. The spectral resolution in the measurements was set to 0.5 nm. The plane of polarization could be selected with a polarizer in the collimated beam path between the two parabolic mirrors.

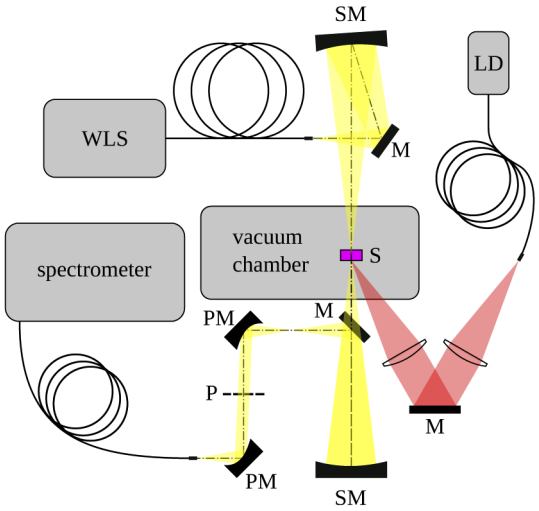

Fig. 1. Schematic of the measurement setup: LD. . . fiber coupled laser diode, M. . . plane mirror, P. . . polarizer, PM. . . off axis parabolic mirror, S. . . sample (mounted in cryostat), SM. . . spherical mirror with radius of 300 mm, WLS. . . fiber coupled white light source.

For fluorescence and lifetime measurements the sample was excited using a fiber coupled laser diode (LD), which was focused onto the sample's surface under an angle with respect to the beam path of the transmitted white light. The pump spot was aligned to intersect with the analysis beam path on the sample's surface. This ensures that only light emitted from a small volume close to the sample's surface is collected for the measurement, thus strongly reducing the influence of re-absorption.

The samples were kept in a high vacuum environment to avoid condensation during the measurements at low temperatures. Cooling was achieved with a ST300 flow cryostat (*Janis Research Company, LLC*) operated with liquid nitrogen and a counter heater to stabilize the temperature. Thermal contact was realized by directly clamping the samples to the cold finger using indium foil on the contact surface.

The absorption cross sections σ_a^{ξ} were determined by measuring the transmitted intensity $I_t^{\xi}(\lambda)$ of the white light source in comparison to a previously measured reference intensity $I_{ref}^{\xi}(\lambda)$. Measurements were conducted for each polarization orientation ξ. In case of the bi-axial crystals two individual samples were used to access all three polarization orientations. To compensate for alignment uncertainties after replacing the sample as well as for Fresnel losses, $I_t^{\xi}(\lambda)$ and $I_{ref}^{\xi}(\lambda)$ were normalized to each other at multiple wavelengths both in the non absorbing spectral areas on the short and the long wavelength side of the absorption band. The intermediate normalization

Optical Materials EXPRESS

factors were then determined by a polynomial approximation. Using these normalized intensities, $\sigma_{\mathrm{a}}^{\xi}$ can be obtained with Lambert-Beer's law:

$$\sigma_{\mathrm{a}}^{\xi} = \frac{\ln\left(\frac{I_{\mathrm{ref}}^{\xi}(\lambda)}{I_{\mathrm{f}}^{\xi}(\lambda)}\right)}{N_{\mathrm{dop}} d}. \tag{1}$$

Here, N_{dop} is the sample's doping concentration in cm^{-3} and d is its thickness.

The emission cross sections $\sigma_{\mathrm{e}}^{\xi}$ are obtained by combining the so-called McCumber (MC) or Reciprocity relation and the Füchtbauer-Ladenburg (FL) equation. The MC-relation allows to directly calculate $\sigma_{\mathrm{e}}^{\xi}(\lambda)$ from the previously determined $\sigma_{\mathrm{a}}^{\xi}(\lambda)$ [17,18]:

$$\sigma_{\mathrm{e}}^{\xi} = \sigma_{\mathrm{a}}^{\xi} \cdot \frac{Z_{\mathrm{l}}}{Z_{\mathrm{u}}} \cdot e^{\frac{E_{\mathrm{ZL}} - \frac{hc}{\lambda}}{kT}}. \tag{2}$$

Here k is the Boltzmann constant, h the Planck constant, c the vacuum speed of light and T the temperature. $E_{\mathrm{ZL}} = hc/\lambda_{ZL}$ is the energy of the zero phonon line (ZPL) transition. $Z_{\mathrm{u/l}}$ are the partition functions for the upper ${}^2\mathrm{F}_{\frac{5}{2}}$ (u) and the lower ${}^2\mathrm{F}_{\frac{7}{2}}$ (l) manifold, which are the only manifolds involved in the laser transitions of Yb^{3+}. These are calculated by:

$$Z_{\mathrm{u/l}}(T) = \sum_i d_i \cdot e^{-\frac{E_i}{kT}}. \tag{3}$$

d_i=2 is the degeneracy of the individual energy levels and E_i the corresponding intra-manifold energies in relation to the lowest energetic level within the corresponding manifold. The energies E_{l} for the lower and E_{u} for the upper manifolds for the investigated materials can be found in Table 2.

Table 2. Energy levels and zero phonon line positions of the investigated laser materials as used in the McCumber relation. The according sources are noted behind the host materials.

host	E_l [cm^{-1}]	E_u [cm^{-1}]	λ_{ZL}
KGW [19,20]	0, 163, 385, 535	10188, 10471, 10682	981.5 nm
KYW [19]	0, 169, 407, 568	10187, 10476, 10695	981.6 nm
YAP [21]	0, 209, 341, 590	10220, 10410, 10730	978.5 nm
YLF [22]	0, 218, 248, 485	10293, 10416, 10554	971.5 nm

The FL-equation uses the normalized line-shape of the optical transition $g_{\lambda}^{\xi}(\lambda)$ to determine $\sigma_{\mathrm{e}}^{\xi}(\lambda)$:

$$\sigma_{\mathrm{e}}^{\xi}(\lambda) = \frac{\lambda^2}{8\pi n^2 \tau_{\mathrm{rad}}} \cdot g_{\lambda}^{\xi}(\lambda) \tag{4}$$

n is the refractive index of the laser medium, which for simplicity reasons we assume as the mean value of all polarization axes in each birefringent crystal as given in Table 1. τ_{rad} is the radiative lifetime of the excited state. This value is not directly accessible through measurement, since the fluorescence decay is influenced e.g. by re-absorption or non radiative decay mechanisms. Therefore, this parameter is treated as an unknown variable that should be similar to τ_{f}. $g_{\lambda}^{\xi}(\lambda)$ can be obtained from the polarized fluorescence intensity $I_{\mathrm{f}}^{\xi}(\lambda)$:

$$g_{\lambda}^{\xi}(\lambda) = \frac{\frac{\lambda^3}{c} \cdot I_{\mathrm{f}}^{\xi}(\lambda)}{\frac{1}{3} \cdot \sum_j \int_{\lambda_{\mathrm{min}}}^{\lambda_{\mathrm{min}}} \lambda I_{\mathrm{f}}^{\xi_j}(\lambda) \mathrm{d}\lambda} \tag{5}$$

The denominator contains the sum over all three polarization axes. For a uni-axial material the σ-polarization needs to be used twice.

Optical Materials EXPRESS

Within our setup, an absolute measurement of the fluorescence intensity would suffer from significant inaccuracies, due to the alignment sensitivity in between the individual measurements. Therefore, the denominator in Eq. (5) in combination with τ_{rad} is treated as a variable during data processing.

Based on the absorption measurement, the MC-relation yields accurate results in spectral areas, where $\sigma_{\mathrm{a}}^{\xi}(\lambda)$ can be measured with high signal to noise ratio. In contrary the $\sigma_{\mathrm{e}}^{\xi}(\lambda)$ obtained by the FL-formalism will have significant errors in such spectral regions due to re-absorption, while it features high reliability for low absorbing areas. Therefore, the variables in the FL-formalism were determined by overlapping the results of both methods in a spectral area with low but accurately measurable absorption. The final $\sigma_{\mathrm{e}}^{\xi}(\lambda)$ are generated by selecting the results from either method depending on which leads to the more accurate results.

After retrieving $\sigma_{\mathrm{e}}^{\xi}(\lambda)$ according to this method, we can now use the FL-formalism to calculate τ_{rad}, which together with the denominator of Eq. (5) was used as an arbitrary variable to overlap the results from both methods with each other. As the denominator in Eq. (5) is the same for all three polarization axes, one obtains for $I_{\mathrm{f}}^{\xi}(\lambda)$:

$$I_{\mathrm{f}}^{\xi}(\lambda) = a \cdot \frac{\sigma_{\mathrm{e}}^{\xi}(\lambda)}{\lambda^5} \tag{6}$$

Here, a is a constant for scaling the total intensity. As long as a has the same value for all polarizations the relative intensities would be scaled to a common total emission. Therefore, τ_{rad} can be calculated by transforming Eq. (4):

$$\tau_{\mathrm{rad}} = \frac{3}{8\pi n^2 c} \cdot \frac{1}{\sum_j \int_{\lambda_{\mathrm{min}}}^{\lambda_{\mathrm{min}}} \frac{\sigma_{\mathrm{e}}^{\xi}(\lambda)}{\lambda^4} \mathrm{d}\lambda} \tag{7}$$

3. Cross sections

The resulting cross sections for Yb:KGW and Yb:KYW are shown in Figs. 3 and 2 respectively. Comparing the results for Yb:KGW with data measured at room temperature from the literature [23], our data is in good agreement. Both materials show very similar spectra both in emission and in absorption. Likewise with varying temperature both materials behave in the same way. Therefore, it should be possible to switch between both materials within a laser setup without significant changes in the laser performance.

In comparison to room temperature the tungstates show a strong increase of about a factor of two to three for the according major emission peak at 80 K in each polarization axis. This is accompanied by a decrease in bandwidth. At 80 K the residual full width at half maximum (FWHM) bandwidth for $\sigma_{\mathrm{e}}^{\xi}(\lambda)$ is ≈6 nm and centered at 1023 nm for the N_{m} and N_{g}-polarizations and 5 nm centered at 1029.5 nm for the N_{p}-polarization. In comparison to room temperature, where broad emission bands dominate, this limits the material's capability for ultra-short pulse amplification or generation, though sub 500 fs pulses should still be feasible with some effort, especially for N_{m} and N_{g}-polarizations. As re-absorption is significantly reduced for low temperatures, especially the emission line in N_{m} polarization at 1023 nm becomes attractive for laser operation. The peak emission cross section of $8.5 \cdot 10^{-20}$ cm^2 is about four times higher than for Yb:YAG's 1030 nm emission at room temperature, but still features a comparable bandwidth and a lower quantum defect.

With respect to the suitability of the absorption cross sections for laser diode pumping, the absolute values reveal only limited information, since the spectral width of the actual pump source always needs to be considered. Therefore, we numerically calculated the product of the material length d in cm and its doping concentration c_{a} in at.% for absorbing 90 % of the pump beam with a Gaussian spectral distribution. For this we neglected saturation effects using Lambert-Beer's

Optical Materials EXPRESS

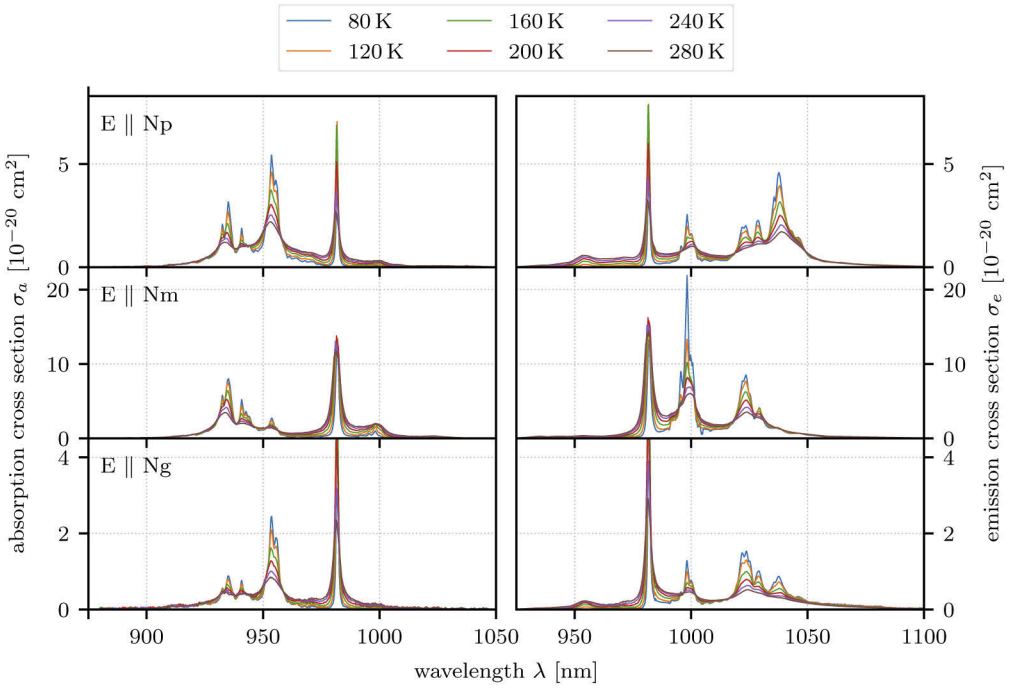

Fig. 2. Polarized absorption (left) and emission cross sections (right) for Yb:KYW at different temperatures. The according polarization is noted in the upper left corner of the graph.

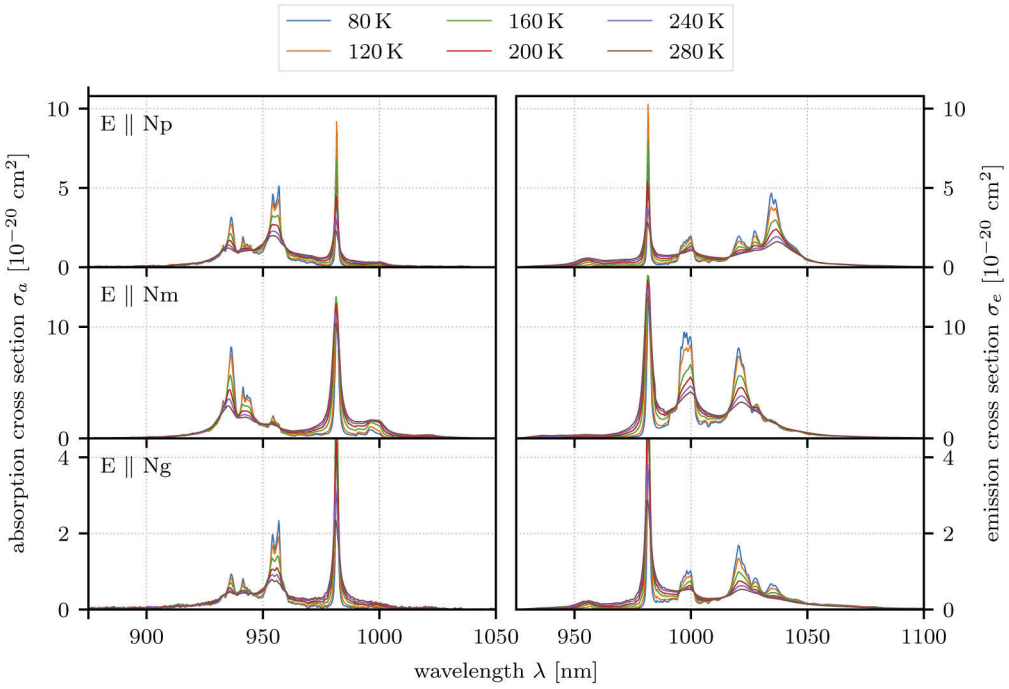

Fig. 3. Polarized absorption (left) and emission cross sections (right) for Yb:KGW at different temperatures. The according polarization is noted in the upper left corner of the graph.

Optical Materials EXPRESS

law. For more details about this we would like to refer to our previous publication [13] The results are shown as a function of the pump's central wavelength λ_p and $1/e^2$ half-bandwidth for each polarization for room temperature and 100 K in Figs. 4(a) for Yb:KGW and 4(b) for Yb:KYW.

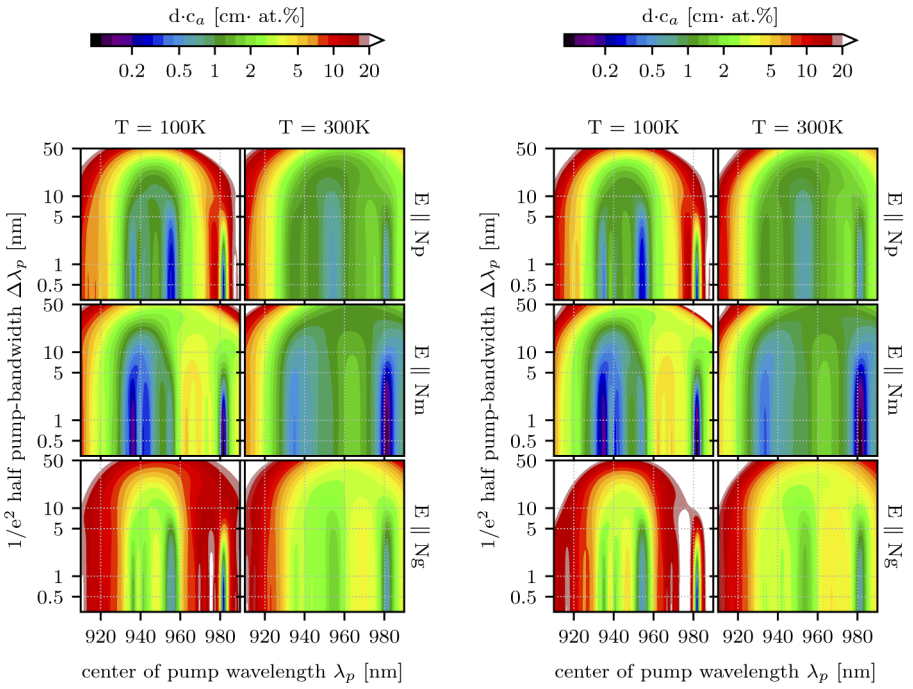

(a) KGW (b) KYW

Fig. 4. Material length for 90% absorption for (a) Yb:KGW and (b) Yb:KYW as a function of the pump's central wavelength λ_p and $1/e^2$ half-bandwidth for each polarization (from top to bottom: N_p, N_m, N_g) at 100 K (left) and room temperature (right).

In principle both tungstates offer two absorption bands that can be used for excitation. One ranges – with some internal structure – from about 930 nm to 960 nm and is therefore compatible with 940 nm pump sources used in Yb:YAG. In this band the use of relatively broad-band pump sources is possible, with up to approximately 10 nm half-bandwidth. Only if the higher values of σ_a^{ξ} in the individual peaks in the low temperature range are to be used, sources with accordingly narrow bandwidth are necessary. The second interesting excitation wavelength is the zero phonon line at 981.5 nm, which allows the operation with reduced quantum defect. To access this absorption line a pump source of less than 5 nm half-bandwidth is required at room temperature. For 100 K the half-bandwidth should be less than 2 nm. Due to the limited spectral resolution of 0.5 nm in our setup the absolute height for the ZPL transition could not be fully resolved at the lowest temperatures.

The retrieved cross sections for Yb:YAP are shown in Fig. 5. A comparison with values from the literature that are available at room temperature [7] shows a good agreement with our data.

The typical wavelength range for ytterbium around 1030 nm is only represented with a relatively weak feature, most pronounced in the b-polarization. Nevertheless, as the spectrum is smooth over a broad range, the material found some application for the generation of ultra-short pulses [7] in this spectral range. In a- and c- polarization σ_a^{ξ} undergoes only minor changes when cooled to 80 K for these wavelengths. However, in the b-polarization the peak cross section

Optical Materials EXPRESS

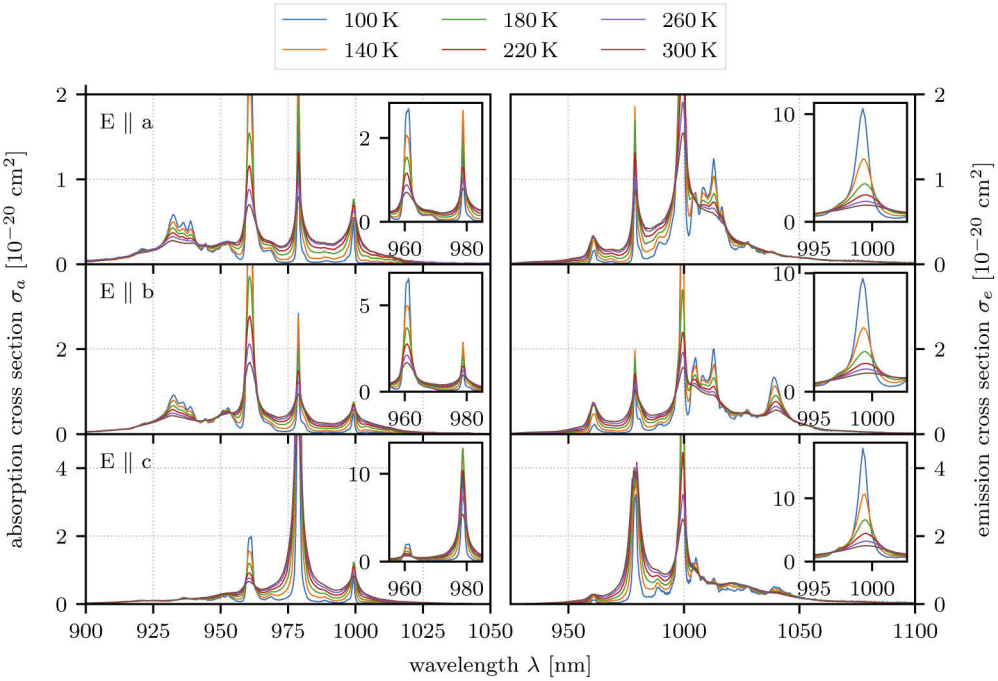

Fig. 5. Polarized absorption (left) and emission cross sections (right) for Yb:YAP at different temperatures. Each polarization is noted in the upper left corner of the according absorption graph. The insets use a different scale to visualize the major peaks.

centered at 1039 nm is about doubled and features a residual FWHM of approximately 5 nm that could be useful for ultra-fast lasers.

The major emission features of Yb:YAP are found in the range from 995 nm to 1015 nm. The peak at 999.2 nm has the highest cross section (see insets in Fig. 5). When cooled to 100 K its peak value is increased approximately by a factor of seven in all polarization axes. In combination with the strongly reduced re-absorption at low temperature this wavelength can be an attractive laser operation wavelength for this material, featuring a low quantum defect. The peak value at 100 K corresponds to more than four times the emission cross section of Yb:YAG at room temperature, and hence promises also a relatively high gain and reasonable saturation fluence for pulsed laser amplifiers.

To evaluate the compatibility for diode pumping an equivalent evaluation as for the tungstates is shown in Fig. 6. In a- and b-polarization a broad absorption band between 930 nm and 940 nm allows compatibility with standard diode pump engines otherwise used with Yb:YAG. A higher absorption can be obtained at the absorption line at 961 nm, though at 100 K a source with less than 2 nm half-bandwidth is required. Also zero phonon line pumping is an option at 978.5 nm but with even higher restrictions according to the half-bandwidth of the pump source, which should be below 1 nm. Again, as in the case of the tungstates, the ZPL was not fully resolved for the lowest temperature measurements to give accurate values of its maximum height and bandwidth.

As a uni-axial fluoride crystal Yb:YLF is quite different when compared to the other investigated materials. Nevertheless, the overall spectral characteristics are quite similar. The determined values for σ_a^{ξ} and σ_e^{ξ} are shown in Fig. 7. The measured values are in good agreement with the values presented by [24] despite the values for σ_e^{σ}. We determined the latter ones to be about half the value given by Kawanaka et al. Further comparison with data in [25] yields a

Optical Materials EXPRESS

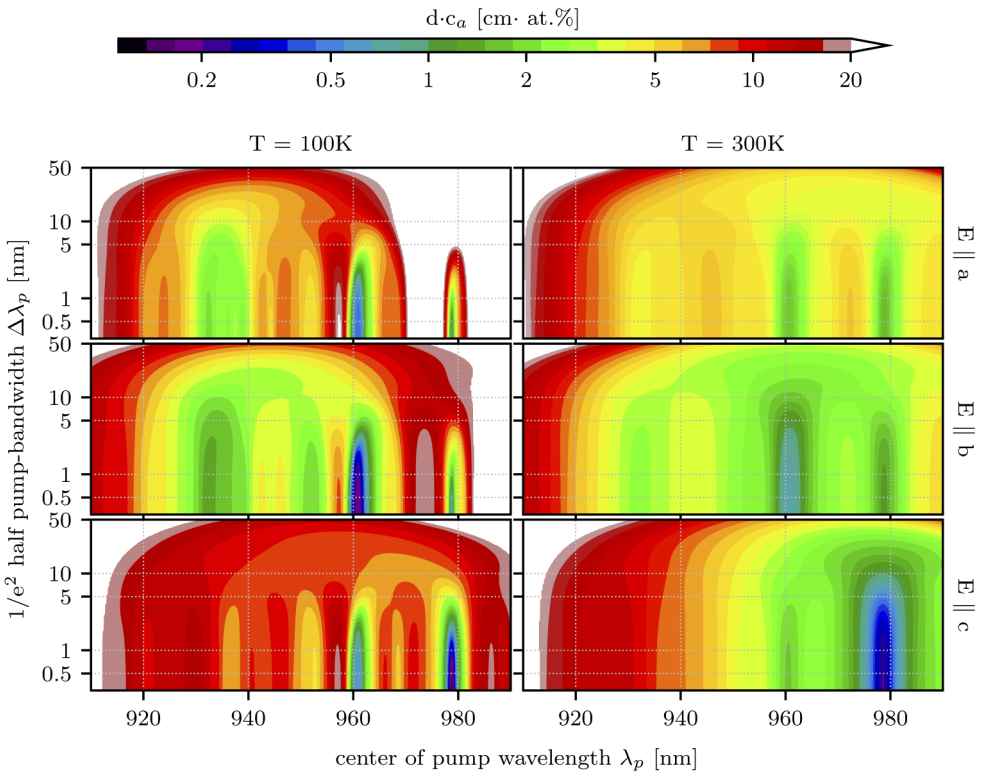

Fig. 6. 90 % absorption length for Yb:YAP as a function of the pump's central wavelength λ_p and $1/e^2$-half-bandwidth for each polarization (from top to bottom: a, b, c) at 100 K (left) and room temperature (right).

good agreement for both polarizations at room temperature. Therefore, we will assume that the determined values are correct.

In π-polarization the peak height at 1020 nm is increased from $0.83{\cdot}10^{-20}$ cm^2 at room temperature to $1.95{\cdot}10^{-20}$ cm^2 at 80 K. At room temperature the structure of the peak extends on the short wavelength side down to ≈1000 nm and reaches its half value on the long wavelength side at 1025 nm. At 80 K it is a well-defined peak with a FWHM bandwidth of 4 nm. In σ-polarization the peak cross section at room temperature is increased from $3.9{\cdot}10^{-20}$ cm^2 to $8.8\cdot10^{-20}$ cm^2 at 80 K. The peak wavelength is at 1018 nm and therefore slightly shorter than for π-polarization. The general spectral characteristic of the emission peak is similar to π-polarization, though the bandwidth is significantly larger. At room temperature the half value is reached at 1026 nm on the long wavelength side. At 80 K the remaining FWHM neglecting the side peak on the blue side is 10 nm. As the peak features a plateau region it can be interesting for ultra-short pulse lasers.

In π-polarization another strong emission line can be found at 993 nm. For low temperatures the line breaks up into a double line, while the peak cross section is strongly increased from $1.2{\cdot}10^{-20}$ cm^2 at room temperature to $9.4{\cdot}10^{-20}$ cm^2 for the line centered at 995.5 nm and $6.5{\cdot}10^{-20}$ cm^2 at 992.75 nm. Due to re-absorption this line is complicated to be used at room temperature, though efficient laser operation has already been demonstrated [10]. Mainly due to the drastic increase of σ_e^{π} and the reduced re-absorption at low temperatures it becomes an attractive laser transition, with low quantum defect in a quite uncommon wavelength range, which supports high power laser operation [26].

Optical Materials EXPRESS

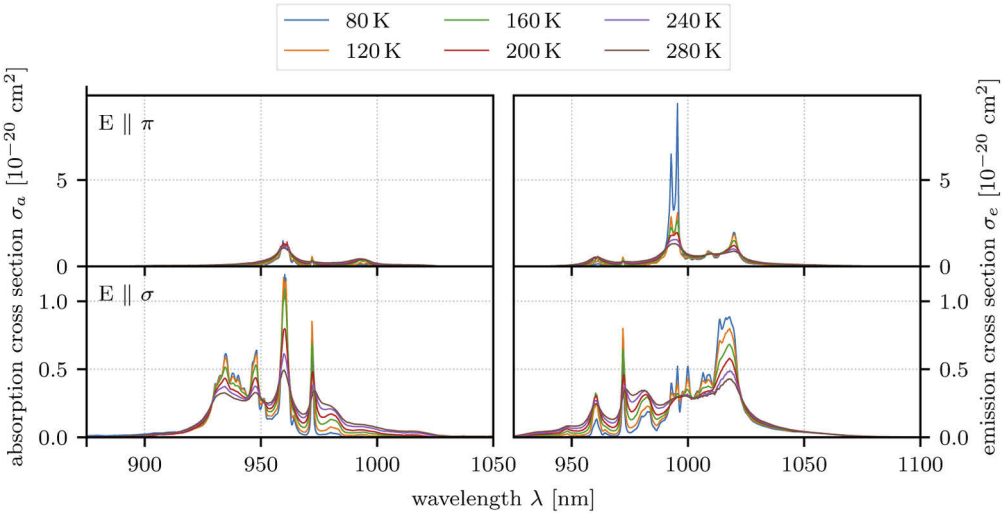

Fig. 7. Polarized absorption (left) and emission cross sections (right) for Yb:YLF at different temperatures. The according polarization is noted in the upper left corner of each absorption graph.

The ZPL at 971.5 nm is only visible as a relatively small peak. It is prominent in the σ-polarization and will most likely not practically useful for laser operation. Similar to the case of the other samples its bandwidth becomes too small to be fully resolved at the lowest temperatures in our setup.

As for the other materials, we calculated the 90 % absorption length as a function of λ_p and $\Delta\lambda_p$ in Fig. 8. The main absorption peak is situated close to the ZPL at 960 nm. The peak

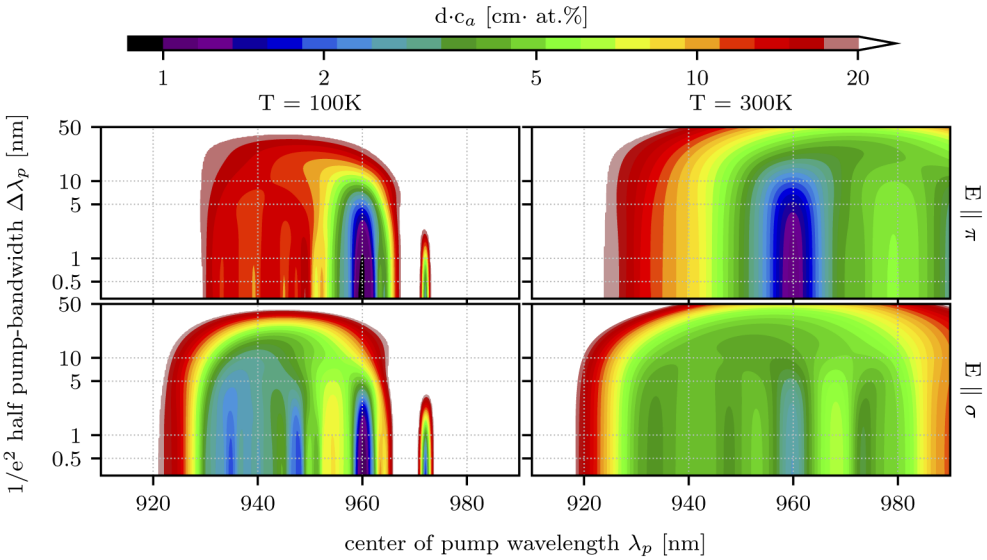

Fig. 8. 90 % absorption length for Yb:YLF as a function of the pump's central wavelength λ_p and $1/e^2$-bandwidth for each polarization (from top to bottom: π, σ) at 100 K (left) and room temperature (right).

Optical Materials EXPRESS

features a higher absorption in π-polarization and can be well accessed with a pump source of up to approximately 5 nm half-bandwidth. The bandwidth and absorption length for this spectral line is nearly constant over the measured temperature range. If a broader pump source is to be used the band ranging from 930 nm to 950 nm in σ-polarisation is an option that would also be compatible with standard 940 nm pump sources. The actual ZPL is rather weak and narrow and therefore not well-suited for diode pumping.

4. Fluorescence lifetimes

Lifetimes have been determined both by direct measurement of the fluorescence decay under pulsed excitation and from the spectral measurements with the formalism described in section 2.

Though carried out in the re-absorption minimized setup, the result from the direct measurement using a photo diode (DET36A/M, *Thorlabs Inc.*) needs to be interpreted as a fluorescence lifetime τ_f, since remaining re-absorption and other effects like quenching may influence the decay curve. Measurements were carried out at multiple temperatures and the decay was fitted with a single exponential decay to determine τ_f. With this method a good overlap of the fitting function was obtained for all samples independent of the temperature. The results for τ_f with according 95 % confidence bands for the fit parameter are given in Fig. 9 as a function of temperature for all investigated materials.

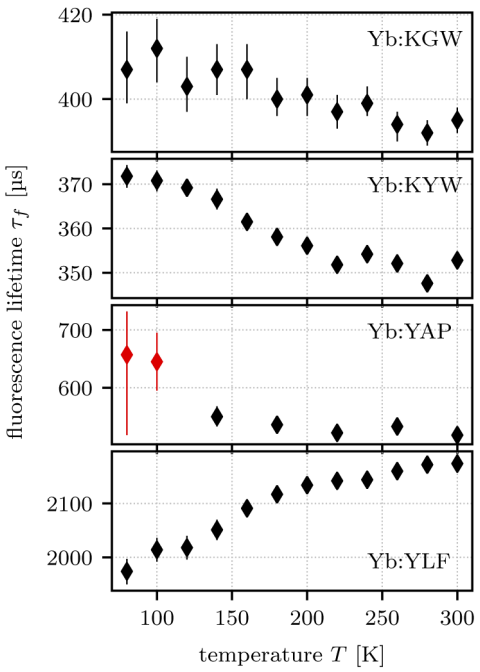

Fig. 9. Results for τ_f obtained by fitting a single exponential decay model to the measured fluorescence decay curves under pulsed excitation. The error bars indicate the 95 % confidence bands of the according fit. Data points in red are neglected for further processing due to their relatively high uncertainty.

For Yb:KGW only a weak tendency to a longer τ_f at lower temperatures can be seen. In case of Yb:KYW this tendency is much clearer, due to a better signal to noise ratio during our measurements. For both materials the overall variation of τ_f is in the range of less than ±5 %. The slight increase of τ_f for lower temperatures might be attributed to a reduction of quenching. Comparing τ_f to the values for τ_{rad} determined from the spectra (cf. Table 3), τ_f is about 30 %

Optical Materials EXPRESS

longer, which indicates a still significant influence of re-absorption in our measurements, caused by the high doping concentration of our samples in combination with the large cross sections. Comparing τ_{rad} with other values from the literature our values are ≈10 % longer, which is a reasonable agreement, given the different means of measurement. Therefore, this is also a good validation for the cross sections presented in section 3.

Table 3. Retrieved lifetimes of the samples and comparison to data from the literature. τ_f... fluorescence life time, τ_{rad}... radiative life time. *The radiative lifetimes where calculated from the emission cross sections according to Eq. (7)

host	τ_f	τ_{rad}
KGW	401±10 µs	272±14 µs *
		242 µs [28]
KYW	359±12 µs	260±21 µs *
		234 µs [28]
YAP	532±16 µs	594±75 µs *
		600 µs [21]
YLF	2100±100 µs	2040±180 µs *
		2210 µs [27]

For Yb:YAP, the measured values for τ_f are nearly constant over temperature, except the values for 80 K and 100 K. However, the low temperature measurement also suffered from a relatively low signal and therefore greater uncertainty. Hence, we will neglect these in the following. Comparing τ_f and τ_{rad}, both are matching within the error margins, also the comparison to values from the literature especially for τ_{rad} shows a good agreement, which also validates our cross section data.

In case of Yb:YLF τ_f is slightly shorter at lower temperatures, which could be attributed to re-absorption caused by the relatively high doping concentration of our sample (cf. table 1). With decreasing temperature the overlap of absorption and emission is reduced, which also reduces the amount of radiation trapping. Therefore, the low temperature value of τ_f of 2.0 ms should be considered closest to τ_{rad}. This value also compares well with the value for τ_{rad} retrieved from the spectra measurements. Comparing to the literature value our value for τ_{rad} is slightly lower, but still within the error margin of 20 % the authors of [27] mention. Therefore, the retrieved lifetimes further support the validity of the cross sections determined in section 3.

5. Conclusion

We presented measurements of the absorption and emission cross sections for Yb:KGW, Yb:KYW and Yb:YLF in the temperature range from 80 K to 280 K and Yb:YAP between 100 K and 300 K. Our results for room temperature are in good agreement with data found in the literature.

The tungstates where found to have nearly identical spectral properties. The height of major emission peaks centered at 1023 nm and 1029.5 nm with respect to polarization are approximately doubled by cooling the sample to 80 K when compared to results at room temperature. Though the emission bandwidth is significantly decreased at lower temperature, the materials should still support the amplification of pulses shorter than 500 fs.

Yb:YAP showed only a weak dependency on temperature for the emission bands starting from ≈1010 nm. Only in b-polarization a significant peak emerged for lower temperatures with about the doubled peak cross section at 80 K compared to room temperature.

Like the aforementioned laser media, Yb:YLF also showed an increase of the peak emission cross section in the major emission band at ≈1020 nm by an factor of approximately two when

Optical Materials EXPRESS

cooling from room temperature down to to 80 K. In σ-polarization the remaining bandwidth at 80 K is 10 nm and therefore still broad enough for ultrashort pulse amplification.

To evaluate the potential of the measured materials to be excited by laser diode pump engines the product of the material length d in cm and its doping concentration c_a in at.% for absorption of 90 % of pump beam with Gaussian spectral distribution was calculated and plotted as a function of the pump's central wavelength λ_p and $1/e^2$ half-bandwidth.

All tested materials also showed a strong increase of emission bands at ≈1000 nm for low temperatures, while re-absorption is suppressed. These materials are therefore especially interesting for low quantum defect operation, which would enable lower heat load and higher output power. Especially Yb:YAP is promising for such an operation scheme due to relatively high cross sections. Additional measurements of the fluorescence lifetime and the determination of the radiative lifetime from the determined emission cross sections showed good agreement with data from the literature, which also supported our data.

Funding

Laserlab-Europe (654148); Bundesministerium für Bildung und Forschung (03VNE2068D, 03Z1H531, 03ZIK445, 05P15SJFA1); Thüringer Ministerium für Bildung, Wissenschaft und Kultur (2016FE9058).

Disclosures

The authors declare no conflicts of interest.

References

1. G. R. Holtom, "Mode-locked Yb:KGW laser longitudinally pumped by polarization-coupled diode bars," Opt. Lett. **31**(18), 2719 (2006).
2. G. Paunescu, J. Hein, and R. Sauerbrey, "100-fs diode-pumped Yb:KGW mode-locked laser," Appl. Phys. B **79**(5), 555–558 (2004).
3. R. Akbari, K. A. Fedorova, E. U. Rafailov, and A. Major, "Diode-pumped ultrafast Yb:KGW laser with 56 fs pulses and multi-100 kW peak power based on sesam and kerr-lens mode locking," Appl. Phys. B **123**(4), 123 (2017).
4. F. Wagner, C. P. Jo ao, J. Fils, T. Gottschall, J. Hein, J. Körner, J. Limpert, M. Roth, T. Stöhlker, and V. Bagnoud, "Temporal contrast control at the PHELIX petawatt laser facility by means of tunable sub-picosecond optical parametric amplification," Appl. Phys. B **116**(2), 429–435 (2014).
5. R. L. Aggarwal, D. J. Ripin, J. R. Ochoa, and T. Y. Fan, "Measurement of thermo-optic properties of $Y_3Al_5O_{12}$, $Y_3Al_5O_{12}$, $YAlO_3$, $LiYF_4$, $LiLuF_4$, BaY_2F_8, $KGd(WO_4)_2$, and $KY(WO_4)_2$ laser crystals in the 80-300 K temperature range," J. Appl. Phys. **98**(10), 103514 (2005).
6. K. Ogawa, Y. Akahane, M. Aoyama, K. Tsuji, S. Tokita, J. Kawanaka, H. Nishioka, and K. Yamakawa, "Multi-millijoule, diode-pumped, cryogenically-cooled Yb:$KY(WO_4)_2$ chirped-pulse regenerative amplifier," Opt. Express **15**(14), 8598 (2007).
7. V. E. Kisel, S. V. Kurilchik, A. S. Yasukevich, S. V. Grigoriev, S. A. Smirnova, and N. V. Kuleshov, "Spectroscopy and femtosecond laser performance of Yb^{3+}:$YAlO_3$ crystal," Opt. Lett. **33**(19), 2194–2196 (2008).
8. N. Coluccelli, G. Galzerano, L. Bonelli, A. Di Lieto, M. Tonelli, and P. Laporta, "Diode-pumped passively mode-locked Yb:YLF laser," Opt. Express **16**(5), 2922 (2008).
9. F. Pirzio, L. Fregnani, A. Volpi, A. D. Lieto, M. Tonelli, and A. Agnesi, "87 fs pulse generation in a diode-pumped semiconductor saturable absorber mirror mode-locked Yb:YLF laser," Appl. Opt. **55**(16), 4414–4417 (2016).
10. N. Ter-Gabrielan, V. Fromzel, T. Sanamyan, and M. Dubinskii, "Highly-efficient Q-switched Yb:YLF laser at 995 nm with a second harmonic conversion," Opt. Mater. Express **7**(7), 2396 (2017).
11. M. Kahle, J. Körner, J. Hein, and M. C. Kaluza, "Performance of a quantum defect minimized disk laser based on cryogenically cooled Yb:caf 2," Opt. Laser Technol. **92**, 19–23 (2017).
12. J. Körner, C. Vorholt, H. Liebetrau, M. Kahle, D. Klöpfel, R. Seifert, J. Hein, and M. C. Kaluza, "Measurement of temperature-dependent absorption and emission spectra of Yb:YAG, Yb:LuAG, and Yb:CaF_2 between 20 °C and 200 °C and predictions on their influence on laser performance," J. Opt. Soc. Am. B **29**(9), 2493 (2012).
13. J. Körner, V. Jambunathan, J. Hein, R. Seifert, M. Loeser, M. Siebold, U. Schramm, P. Sikocinski, A. Lucianetti, T. Mocek, and M. C. Kaluza, "Spectroscopic characterization of Yb^{3+}-doped laser materials at cryogenic temperatures," Appl. Phys. B **116**(1), 75–81 (2014).
14. M. Pujol, M. Rico, C. Zaldo, R. Solé, V. Nikolov, X. Solans, M. Aguiló, and F. Díaz, "Crystalline structure and optical spectroscopy of Er^{3+}-doped $KGd(WO_4)_2$ single crystals," Appl. Phys. B **68**(2), 187–197 (1999).

Optical Materials EXPRESS

15. X. Mateos, R. Solé, J. Gavaldá, M. Aguiló, J. Massons, and F. Díaz, "Crystal growth, optical and spectroscopic characterisation of monoclinic $KY(WO_4)_2$ co-doped with Er^{3+} and Yb^{3+}," Opt. Mater. **28**(4), 423–431 (2006).
16. L. DeLoach, S. Payne, L. Chase, L. Smith, W. Kway, and W. Krupke, "Evaluation of absorption and emission properties of Yb^{3+} doped crystals for laser applications," IEEE J. Quantum Electron. **29**(4), 1179–1191 (1993).
17. D. E. McCumber, "Einstein relations connecting broadband emission and absorption spectra," Phys. Rev. **136**(4A), A954–A957 (1964).
18. R. M. Martin and R. S. Quimby, "Experimental evidence of the validity of the mccumber theory relating emission and absorption for rare-earth glasses," J. Opt. Soc. Am. B **23**(9), 1770–1775 (2006).
19. N. V. Kuleshov, A. A. Lagatsky, A. V. Podlipensky, V. P. Mikhailov, and G. Huber, "Pulsed laser operation of Yb-doped $KY(WO_4)_2$ and $KGd(WO_4)_2$," Opt. Lett. **22**(17), 1317 (1997).
20. C. Cascales, "Evaluation of crystal field effects of Yb^{3+} in monoclinic $KGd(WO_4)_2$ and $KYb(WO_4)_2$ laser crystals. comparison with disordered tetragonal $NaGd(WO_4)_2$ crystals," The Journal of the Argentine Chemical Society **97**, 25–38 (2009).
21. G. Boulon, Y. Guyot, H. Canibano, S. Hraiech, and A. Yoshikawa, "Characterization and comparison of Yb^{3+}-doped $YAlO_3$ perovskite crystals (Yb:YAP) with Yb^{3+}-doped $Y_3Al\_5O_{12}$ garnet crystals (Yb:YAG) for laser application," J. Opt. Soc. Am. B **25**(5), 884 (2008).
22. A. Bensalah, Y. Guyot, M. Ito, A. Brenier, H. Sato, T. Fukuda, and G. Boulon, "Growth of Yb^{3+}-doped ylif4 laser crystal by the czochralski method. attempt of Yb^{3+} energy level assignment and estimation of the laser potentiality," Opt. Mater. **26**(4), 375–383 (2004).
23. M. Zhou, D. X. Cao, M. Z. Wang, X. F. Wang, and Y. M. Luo, "Polarized fluorescence spectra analysis of Yb^{3+}:$KGd(WO_4)_2$," Opt. Commun. **282**(20), 4109–4113 (2009).
24. J. Kawanaka, H. Nishioka, N. Inoue, and K. Ueda, "Tunable continuous-wave Yb:YLF laser operation with a diode-pumped chirped-pulse amplification system," Appl. Opt. **40**(21), 3542–3546 (2001).
25. M. Vannini, G. Toci, D. Alderighi, D. Parisi, F. Cornacchia, and M. Tonelli, "High efficiency room temperature laser emission in heavily doped Yb:YLF," Opt. Express **15**(13), 7994–8002 (2007).
26. L. E. Zapata, D. J. Ripin, and T. Y. Fan, "Power scaling of cryogenic Yb:$LiYF_4$ lasers," Opt. Lett. **35**(11), 1854–1856 (2010).
27. L. D. Deloach, S. A. Payne, L. L. Chase, L. K. Smith, W. L. Kway, and W. F. Krupke, "Evaluation of absorption and emission properties of Yb^{3+} doped crystals for laser applications," IEEE J. Quantum Electron. **29**(4), 1179–1191 (1993).
28. A. S. Yasyukevich, V. G. Shcherbitskii, V. E. Kisel, A. V. Mandrik, and N. V. Kuleshov, "Integral method reciprocity in the spectroscopy of laser crystals with impurity centers," J. Appl. Spectrosc. **71**(2), 202–208 (2004).